LETTER

doi:10.1038/nature14964

Conventional superconductivity at 203 kelvin at high pressures in the sulfur hydride system

A. P. Drozdov[1]*, M. I. Eremets[1]*, I. A. Troyan[1], V. Ksenofontov[2] & S. I. Shylin[2]

A superconductor is a material that can conduct electricity without resistance below a superconducting transition temperature, T_c. The highest T_c that has been achieved to date is in the copper oxide system[1]: 133 kelvin at ambient pressure[2] and 164 kelvin at high pressures[3]. As the nature of superconductivity in these materials is still not fully understood (they are not conventional superconductors), the prospects for achieving still higher transition temperatures by this route are not clear. In contrast, the Bardeen–Cooper–Schrieffer theory of conventional superconductivity gives a guide for achieving high T_c with no theoretical upper bound—all that is needed is a favourable combination of high-frequency phonons, strong electron–phonon coupling, and a high density of states[4]. These conditions can in principle be fulfilled for metallic hydrogen and covalent compounds dominated by hydrogen[5,6], as hydrogen atoms provide the necessary high-frequency phonon modes as well as the strong electron–phonon coupling. Numerous calculations support this idea and have predicted transition temperatures in the range 50–235 kelvin for many hydrides[7], but only a moderate T_c of 17 kelvin has been observed experimentally[8]. Here we investigate sulfur hydride[9], where a T_c of 80 kelvin has been predicted[10]. We find that this system transforms to a metal at a pressure of approximately 90 gigapascals. On cooling, we see signatures of superconductivity: a sharp drop of the resistivity to zero and a decrease of the transition temperature with magnetic field, with magnetic susceptibility measurements confirming a T_c of 203 kelvin. Moreover, a pronounced isotope shift of T_c in sulfur deuteride is suggestive of an electron–phonon mechanism of superconductivity that is consistent with the Bardeen–Cooper–Schrieffer scenario. We argue that the phase responsible for high-T_c superconductivity in this system is likely to be H_3S, formed from H_2S by decomposition under pressure. These findings raise hope for the prospects for achieving room-temperature superconductivity in other hydrogen-based materials.

A search for high- (room)-temperature conventional superconductivity is likely to be fruitful, as the Bardeen–Cooper–Schrieffer (BCS) theory in the Eliashberg formulation puts no apparent limits on T_c. Materials with light elements are especially favourable as they provide high frequencies in the phonon spectrum. Indeed, many superconductive materials have been found in this way, but only a moderately high $T_c = 39$ K has been found in this search (in MgB_2; ref. 11).

Ashcroft[5] turned attention to hydrogen, which has very high vibrational frequencies due to the light hydrogen atom and provides a strong electron–phonon interaction. Further calculations showed that metallic hydrogen should be a superconductor with a very high T_c of about 100–240 K for molecular hydrogen, and of 300–350 K in the atomic phase at 500 GPa (ref. 12). However, superconductivity in pure hydrogen has not yet been found, even though a conductive and probably semimetallic state of hydrogen has been recently produced[13]. Hydrogen-dominated materials such as covalent hydrides SiH_4, SnH_4, and so on might also be good candidates for showing high-T_c superconductivity[6]. Similarly to pure hydrogen, they have high Debye temperatures. Moreover, heavier elements might be beneficial as they contribute to the low frequencies that enhance electron–phonon coupling. Importantly, lower pressures are required to metallize hydrides in comparison to pure hydrogen. Ashcroft's general idea was supported in numerous calculations[7,10] predicting high values of T_c for many hydrides. So far only a low T_c (~17 K) has been observed experimentally[8].

For the present study we selected H_2S, because it is relatively easy to handle and is predicted to transform to a metal and a superconductor at a low pressure $P \approx 100$ GPa with a high $T_c \approx 80$ K (ref. 10). Experimentally, H_2S is known as a typical molecular compound with a rich phase diagram[14]. At about 96 GPa, hydrogen sulphide transforms to a metal[15]. The transformation is complicated by the partial dissociation of H_2S and the appearance of elemental sulfur at $P > 27$ GPa at room temperature, and at higher pressures at lower temperatures[14]. Therefore, the metallization of hydrogen sulphide can be explained by elemental sulfur, which is known to become metallic above 95 GPa (ref. 16). No experimental studies of hydrogen sulphide are known above 100 GPa.

In a typical experiment, we performed loading and the initial pressure increase at temperatures of ~200 K; this is essential for obtaining a good sample (Methods). The Raman spectra of H_2S and D_2S were measured as the pressure was increased, and were in general agreement with the literature data[17,18] (Extended Data Fig. 1). The sample starts to conduct at $P \approx 50$ GPa. At this pressure it is a semiconductor, as shown by the temperature dependence of the resistance and pronounced photoconductivity. At 90–100 GPa the resistance drops further, and the temperature dependence becomes metallic. No photoconductive response is observed in this state. It is a poor metal—its resistivity at ~100 K is $\rho \approx 3 \times 10^{-5}$ ohm m at 110 GPa and $\rho \approx 3 \times 10^{-7}$ ohm m at ~200 GPa.

During the cooling of the metal at pressures of about 100 GPa (Fig. 1a) the resistance abruptly drops by three to four orders of magnitude, indicating a transition to the superconducting state. At the next increase of pressure at low temperatures of $T < 100$ K, T_c steadily increases with pressure. However, at pressures of >160 GPa, T_c increases sharply (Fig. 1b). As higher temperatures of 150–250 K were involved in this pressure range, we supposed that the increase of T_c and the decrease of sample resistance during warming (Fig. 1a) could indicate a possible kinetic-controlled phase transformation. Therefore in further experiments, after loading and after the initial pressure increase at 200 K, we annealed all samples by heating them to room temperature (or above) at pressures of >~150 GPa (Fig. 2a, see also Extended Data Fig. 2). This allowed us to obtain stable results, to compare different isotopes, to obtain the dependence of T_c on pressure and magnetic field, and to prove the existence of superconductivity in our samples as follows. (We note that additional information on experimental conditions are given in the appropriate figure legends.)

[1]Max-Planck-Institut für Chemie, Hahn-Meitner-Weg 1, 55128 Mainz, Germany. [2]Institut für Anorganische Chemie und Analytische Chemie, Johannes Gutenberg-Universität Mainz, Staudingerweg 9, 55099 Mainz, Germany.

*These authors contributed equally to this work.

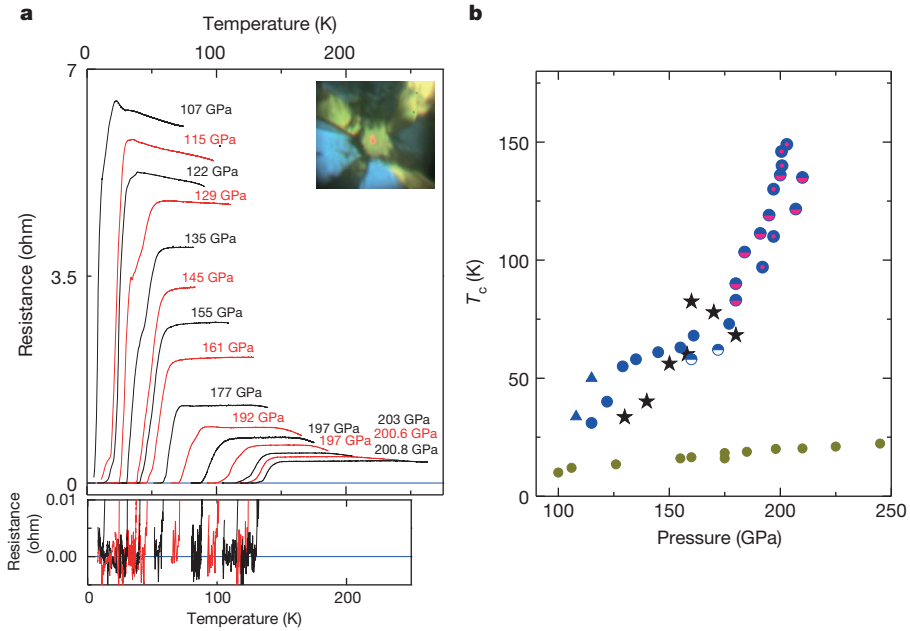

Figure 1 | Temperature dependence of the resistance of sulfur hydride measured at different pressures, and the pressure dependence of T_c. **a**, Main panel, temperature dependence of the resistance (R) of sulfur hydride at different pressures. The pressure values are indicated near the corresponding plots. At first, the sample was loaded at $T \approx 200$ K and the pressure was increased to ~100 GPa; the sample was then cooled down to 4 K. After warming to ~100 K, pressure was further increased. Plots at pressures <135 GPa have been scaled (reduced) as follows—105 GPa, by 10 times; 115 GPa and 122 GPa, by 5 times; and 129 GPa by 2 times—for easier comparison with the higher pressure steps. The resistance was measured with a current of 10 μA. Bottom panel, the resistance plots near zero. The resistance was measured with four electrodes deposited on a diamond anvil that touched the sample (top panel inset). The diameters of the samples were ~25 μm and the thickness was ~1 μm. **b**, Blue round points represent values of T_c determined from **a**. Other blue points (triangles and half circles) were obtained in similar runs. Measurements at $P > \sim 160$ GPa revealed a sharp increase of T_c. In this pressure range the $R(T)$ measurements were performed over a larger temperature range up to 260 K, the corresponding experimental points for two samples are indicated by adding a pink colour to half circles and a centred dot to filled circles. These points probably reflect a transient state for these particular P/T conditions. Further annealing of the sample at room temperature would require stabilizing the sample (Fig. 2a). Black stars are calculations from ref. 10. Dark yellow points are T_c values of pure sulfur obtained with the same four-probe electrical measurement method. They are consistent with literature data[30] (susceptibility measurements) but have higher values at $P > 200$ GPa.

(1) There is a sharp drop in resistivity with cooling, indicating a phase transformation. The measured minimum resistance is at least as low, $\sim 10^{-11}$ ohm m—about two orders of magnitude less than for pure copper (Fig. 1, Extended Data Fig. 3e) measured at the same temperature[19]. (2) A strong isotope effect is observed: T_c shifts to lower temperatures for sulfur deuteride, indicating phonon-assisted superconductivity (Fig. 2b, c). The BCS theory gives the dependence of T_c on atomic mass m as $T_c \propto m^{-\alpha}$, where $\alpha \approx 0.5$. Comparison of T_c values in the pressure range $P > 170$ GPa (Fig. 2c) gives $\alpha \approx 0.3$. (3) T_c shifts to lower temperatures with available magnetic field (B) up to 7 T

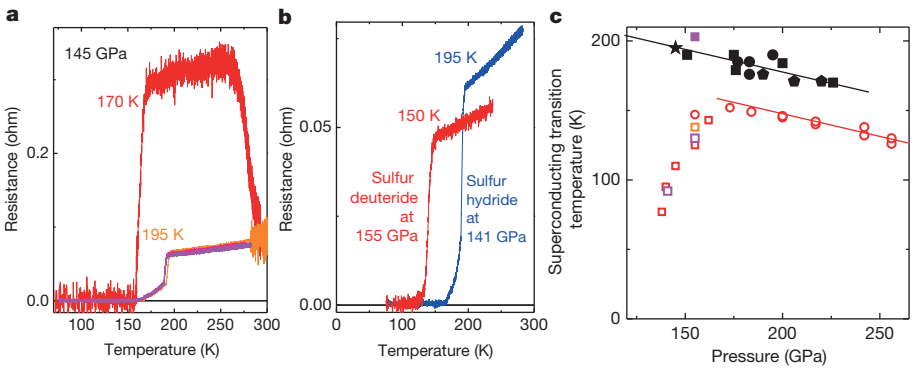

Figure 2 | Pressure and temperature effects on T_c of sulfur hydride and sulfur deuteride. **a**, Changes of resistance and T_c of sulfur hydride with temperature at constant pressure—the annealing process. The sample was pressurized to 145 GPa at 220 K and then cooled to 100 K. It was then slowly warmed at ~1 K min^{-1}; $T_c = 170$ K was determined. At temperatures above ~250 K the resistance dropped sharply, and during the next temperature run T_c increased to ~195 K. This T_c remained nearly the same for the next two runs. (We note that the only point for sulfur deuteride presented in ref. 9 was determined without sample annealing, and T_c would increase after annealing at room temperature.) **b**, Typical superconductive steps for sulfur hydride (blue trace) and sulfur deuteride (red trace). The data were acquired during slow warming over a time of several hours. T_c is defined here as the sharp kink in the transition to normal metallic behaviour. These curves were obtained after annealing at room temperature as shown in **a**. **c**, Dependence of T_c on pressure; data on annealed samples are presented. Open coloured points refer to sulfur deuteride, and filled points to sulfur hydride. Data shown as the magenta point were obtained in magnetic susceptibility measurements (Fig. 4a). The lines indicate that the plots are parallel at pressures above ~170 GPa (the isotope shift is constant) but strongly deviate at lower pressures.

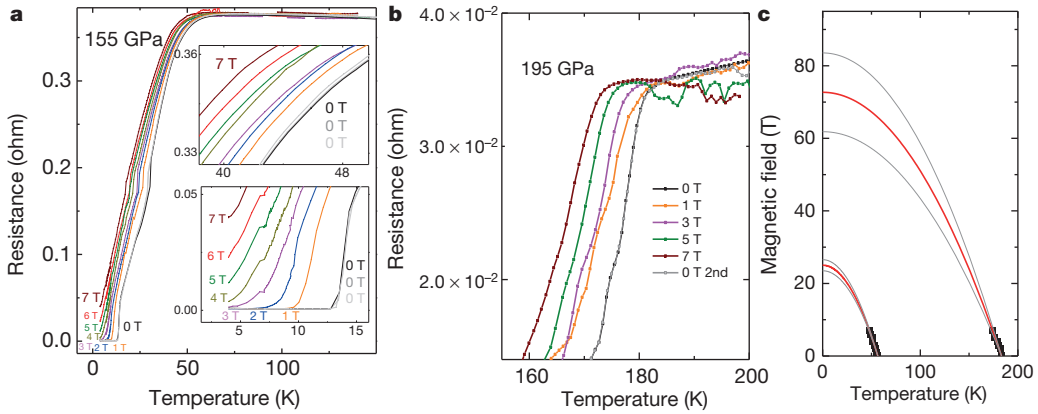

Figure 3 | Temperature dependence of the resistance of sulfur hydride in different magnetic fields. **a**, The shift of the ~60 K superconducting transition in magnetic fields of 0–7 T (colour coded). The upper and lower parts of the transition are shown enlarged in the insets (axes as in main panel). The temperature dependence of the resistance without an applied magnetic field was measured three times: before applying the field, after applying 1, 3, 5, 7 T and finally after applying 2, 4, 6 T (black, grey and dark grey colours). **b**, The same measurements but for the 185 K superconducting transition. **c**, The temperature dependence of the critical magnetic field strengths of sulfur hydride. T_c (black points deduced from **a**, **b**) are plotted for the corresponding magnetic fields. To estimate the critical magnetic field H_c, the plots were extrapolated to high magnetic fields using the formula $H_c(T) = H_{c0}(1 - (T/T_c)^2)$. The extrapolation has been done with 95% confidence (band shown as grey lines).

(Fig. 3). Much higher fields are required to destroy the superconductivity: extrapolation of $T_c(B)$ gives an estimate of a critical magnetic field as high as 70 T (Fig. 3). (4) Finally, in magnetic susceptibility measurements (Fig. 4) a sharp transition from the diamagnetic to the paramagnetic state (Fig. 4a) was observed for zero-field-cooled (ZFC) material. The onset temperature of the superconducting state T_{onset} = 203(1) K, and the width of the superconducting transition is nearly the same as in electrical measurements (Fig. 4a). Magnetization measurements $M(H)$, where H is magnetic field, at different temperatures (Fig. 4c) revealed a pronounced hysteresis indicating type II superconductivity with the first critical field $H_{c1} \approx 30$ mT. The magnetization decreases sharply at temperatures above 200 K showing the onset of superconductivity at 203.5 K, in agreement with the susceptibility measurements (Fig. 4a). A list of key properties of the new superconductor is given in Methods.

We have presented purely experimental evidence of superconductivity in sulfur hydride. However the particular compound responsible for the high T_c is not obvious. The superconductivity measured in the

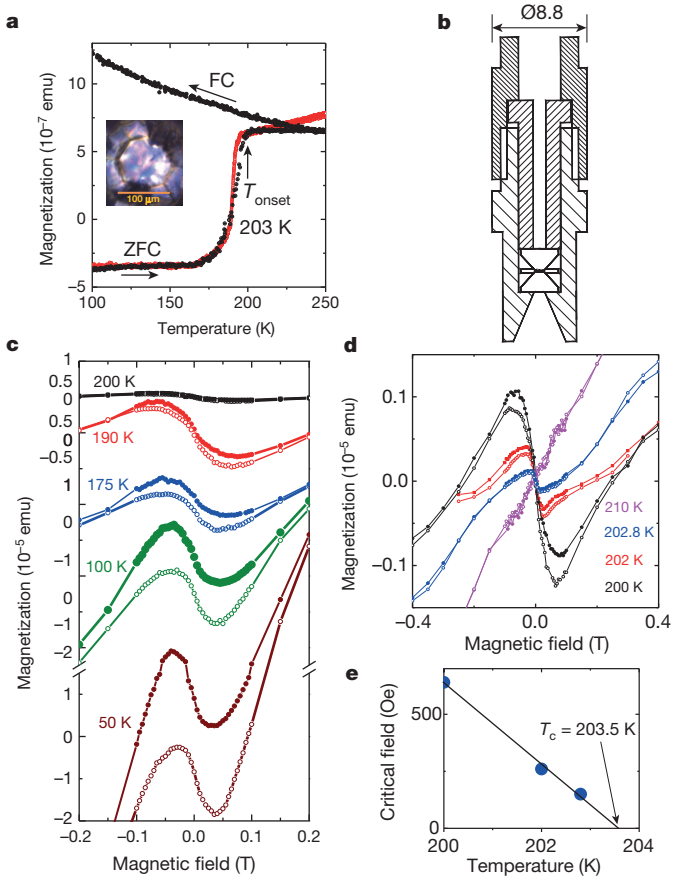

Figure 4 | Magnetization measurements. **a**, Temperature dependence of the magnetization of sulfur hydride at a pressure of 155 GPa in zero-field cooled (ZFC) and 20 Oe field cooled (FC) modes (black circles). The onset temperature is T_{onset} = 203(1) K. For comparison, the superconducting step obtained for sulfur hydride from electrical measurements at 145 GPa is shown by red circles. Resistivity data (T_{onset} = 195 K) were scaled and moved vertically to compare with the magnetization data. Inset, optical micrograph of a sulfur hydride sample at 155 GPa in a $CaSO_4$ gasket (scale bar 100 μm). The high T_{onset} = 203 K measured from the susceptibility can be explained by a significant input to the signal from the periphery of the sample which expanded beyond the culet where pressure is smaller than in the culet centre (T_c increases with decreasing pressure (Fig. 2b)). **b**, Non-magnetic diamond anvil cell (DAC) of diameter 8.8 mm. **c**, Magnetization measurements $M(H)$ of sulfur hydride at a pressure of 155 GPa at different temperatures (given as curve labels). The magnetization curves show hysteresis, indicating a type II superconductor. The magnetization curves are however distorted by obvious paramagnetic input (which is also observed in other superconductors[31]). In our case, the paramagnetic signal is probably from the DAC, but further study of the origin of this input is required. The paramagnetic background increases when temperature is decreased. The minima of the magnetization curves (~35 mT) are the result of the diamagnetic input from superconductivity and the paramagnetic background. The first critical field $H_{c1} \approx 30$ mT can be roughly estimated as the point where magnetization deviates from linear behaviour. At higher fields, magnetization increases due to the penetration of magnetic vortexes. As the sign of the field change reverses, the magnetic flux in the Shubnikov phase remains trapped and therefore the back run (that is, with decreasing field) is irreversible—the returning branch of the magnetic cycle (shown by filled points) runs above the direct one. Hysteretic behaviour of the magnetization becomes more clearly visible as the temperature decreases. **d**, At high temperatures $T > 200$ K, the magnetization decreases sharply. **e**, Extrapolation of the pronounced minima at the magnetization curves to higher temperatures gives the onset of superconductivity at T = 203.5 K.

low-temperature runs (Fig. 1) possibly relates to H_2S, as it is generally consistent with calculations[10] for H_2S: both the value of $T_c \approx 80$ K and its pressure behaviour. However superconductivity with $T_c \approx 200$ K (Fig. 2) does not follow from these calculations. We suppose that it relates to the decomposition of H_2S, as high temperatures are required to reach the high T_c (Fig. 2b). Precipitation of elemental sulfur on decomposition could be expected (which is well known at low pressures of $P < 100$ GPa; ref. 14); however the superconducting transition in elemental sulfur occurs at significantly lower temperatures (Fig. 1b). Another expected product of decomposition of H_2S is hydrogen. However, the strong characteristic vibrational stretching mode from the H_2 molecule was never observed in our Raman spectra (nor was it observed in ref. 14). Therefore we suppose that the dissociation of H_2S is different and involves the creation of higher hydrides, such as $3H_2S \rightarrow H_6S + 2S$ or $2H_2S \rightarrow H_4S + S$. It is natural to expect these reactions, as sulfur can be not only divalent, but also exhibits higher valencies. In fact, calculations[10] indirectly support this hypothesis, as the dissociation $H_2S \rightarrow H_2 + S$ was shown to be energetically very unfavourable. We found further theoretical support in ref. 20. In that work, the van der Waals compound[21] $(H_2S)_2H_2$ was considered, and it was shown that at pressures above 180 GPa it forms an *Im*-3*m* structure with H_3S stoichiometry. The predicted $T_c \approx 190$ K and its pressure dependences are close to our experimental values (Fig. 2c). Our hypothesis of the transformation of H_2S to higher hydrides (in the H_3S stoichiometry each S atom is surrounded by 6 hydrogen atoms) is strongly supported by further calculations[22,23]. All the numerous works based on the *Im*-3*m* structure[23–27] are consistent in their prediction of $T_c > \sim 200$ K, which decreases with pressure. The hydrogen sublattice gives the main contribution to superconductivity[20,25,26]. Inclusion of zero point vibrations and anharmonicity in the calculations[24] corrected the calculated T_c to ~190 K, and the isotope coefficient from $\alpha = 0.5$ to $\alpha = 0.35$—both in agreement with the present work.

The highest T_c of 203 K that we report here has been achieved most probably in H_3S having the *Im*-3*m* structure. It is a good metal; interestingly, there is also strong covalent bonding between H and S atoms in this compound[20]. This is in agreement with the general assumption (see for instance ref. 28) that a metal with high T_c should have strong covalent bonding (as is realized in MgB_2; ref. 29) together with high-frequency modes in the phonon spectrum. This particular combination of bonding type and phonon spectrum would probably provide a good criterion when searching for the materials with high T_c at ambient pressure that are required for applications. There are many hydrogen-containing materials with strong covalent bonding (such as organics) but typically they are insulators. In principle, they could be tuned to a metallic state by doping or gating. Modern methods of structure prediction could facilitate exploration for the desired materials.

Online Content Methods, along with any additional Extended Data display items and Source Data, are available in the online version of the paper; references unique to these sections appear only in the online paper.

Received 25 June; accepted 22 July 2015.
Published online 17 August 2015.

1. Bednorz, J. G. & Mueller, K. A. Possible high T_C superconductivity in the Ba-La-Cu-O system. *Z. Phys. B* **64,** 189–193 (1986).
2. Schilling, A., Cantoni, M., Guo, J. D. &. Ott, H. R. Superconductivity above 130 K in the Hg-Ba-Ca-Cu-O system. *Nature* **363,** 56–58 (1993).
3. Gao, L. *et al.* Superconductivity up to 164 K in $HgBa_2Ca_{m-1}Cu_mO_{2m+2+\delta}$ (m=l, 2, and 3) under quasihydrostatic pressures. *Phys. Rev. B* **50,** 4260–4263 (1994).
4. Ginzburg, V. L. Once again about high-temperature superconductivity. *Contemp. Phys.* **33,** 15–23 (1992).
5. Ashcroft, N. W. Metallic hydrogen: A high-temperature superconductor? *Phys. Rev. Lett.* **21,** 1748–1750 (1968).
6. Ashcroft, N. W. Hydrogen dominant metallic alloys: high temperature superconductors? *Phys. Rev. Lett.* **92,** 187002 (2004).
7. Wang, Y. & Ma, Y. Perspective: Crystal structure prediction at high pressures. *J. Chem. Phys.* **140,** 040901 (2014).
8. Eremets, M. I., Trojan, I. A., Medvedev, S. A., Tse, J. S. & Yao, Y. Superconductivity in hydrogen dominant materials: silane. *Science* **319,** 1506–1509 (2008).
9. Drozdov, A. P., Eremets, M. I. & Troyan, I. A. Conventional superconductivity at 190 K at high pressures. Preprint at http://arXiv.org/abs/1412.0460 (2014).
10. Li, Y., Hao, J., Li, Y. & Ma, Y. The metallization and superconductivity of dense hydrogen sulfide. *J. Chem. Phys.* **140,** 174712 (2014).
11. Nagamatsu, J., Nakagawa, N., Muranaka, T., Zenitani, Y. & Akimitsu, J. Superconductivity at 39 K in magnesium diboride. *Nature* **410,** 63–64 (2001).
12. McMahon, J. M., Morales, M. A., Pierleoni, C. & Ceperley, D. M. The properties of hydrogen and helium under extreme conditions. *Rev. Mod. Phys.* **84,** 1607–1653 (2012).
13. Eremets, M. I. & Troyan, I. A. Conductive dense hydrogen. *Nature Mater.* **10,** 927–931 (2011).
14. Fujihisa, H. *et al.* Molecular dissociation and two low-temperature high-pressure phases of H_2S. *Phys. Rev. B* **69,** 214102 (2004).
15. Sakashita, M. *et al.* Pressure-induced molecular dissociation and metallization in hydrogen-bonded H_2S solid. *Phys. Rev. Lett.* **79,** 1082–1085 (1997).
16. Kometani, S., Eremets, M., Shimizu, K., Kobayashi, M. & Amaya, K. Observation of pressure-induced superconductivity of sulfur. *J. Phys. Soc. Jpn.* **66,** 2564–2565 (1997).
17. Shimizu, H. *et al.* Pressure-temperature phase diagram of solid hydrogen sulfide determined by Raman spectroscopy. *Phys. Rev. B* **51,** 9391–9394 (1995).
18. Shimizu, H., Murashima, H. & Sasaki, S. High-pressure Raman study of solid deuterium sulfide up to 17 GPa. *J. Chem. Phys.* **97,** 7137–7139 (1992).
19. Matula, R. A. Electrical resistivity of copper, gold, palladium, and silver. *J. Phys. Chem. Ref.* **8,** 1147–1298 (1979).
20. Duan, D. *et al.* Pressure-induced metallization of dense $(H_2S)_2H_2$ with high-T_c superconductivity. *Sci. Rep.* **4,** 6968 (2014).
21. Strobel, T. A., Ganesh, P., Somayazulu, M., Kent, P. R. C. & Hemley, R. J. Novel cooperative interactions and structural ordering in H_2S–H_2. *Phys. Rev. Lett.* **107,** 255503 (2011).
22. Duan, D. *et al.* Pressure-induced decomposition of solid hydrogen sulfide. *Phys. Rev. B* **91,** 180502(R) (2015).
23. Bernstein, N., Hellberg, C. S., Johannes, M. D., Mazin, I. I. & Mehl, M. J. What superconducts in sulfur hydrides under pressure, and why. *Phys. Rev. B* **91,** 060511(R) (2015).
24. Errea, I. *et al.* Hydrogen sulfide at high pressure: a strongly-anharmonic phonon-mediated superconductor. *Phys. Rev. Lett.* **114,** 157004 (2015).
25. Flores-Livas, J. A., Sanna, A. & Gross, E. K. U. High temperature superconductivity in sulfur and selenium hydrides at high pressure. Preprint at http://arXiv.org/abs/1501.06336v1 (2015).
26. Papaconstantopoulos, D. A., Klein, B. M., Mehl, M. J. & Pickett, W. E. Cubic H_3S around 200 GPa: an atomic hydrogen superconductor stabilized by sulfur. *Phys. Rev. B.* **91,** 184511 (2015).
27. Akashi, R., Kawamura, M., Tsuneyuki, S., Nomura, Y. & Arita, R. Fully non-empirical study on superconductivity in compressed sulfur hydrides. Preprint at http://arXiv.org/abs/1502.00936v1 (2015).
28. Cohen, M. L. in *BCS: 50 years* (eds Cooper, L. N. & Feldman, D.) 375–389 (World Scientific, 2011).
29. An, J. M. & Pickett, W. E. Superconductivity of MgB_2: covalent bonds driven metallic. *Phys. Rev. Lett.* **86,** 4366–4369 (2001).
30. Gregoryanz, E. *et al.* Superconductivity in the chalcogens up to multimegabar pressures. *Phys. Rev. B* **65,** 064504 (2002).
31. Senoussi, S., Sastry, P., Yakhmi, J. V. & Campbell, I. Magnetic hysteresis of superconducting $GdBa_2Cu_3O_7$ down to 1.8 K. *J. Phys.* **49,** 2163–2164 (1988).

Acknowledgements Support provided by the European Research Council under the 2010 Advanced Grant 267777 is acknowledged. We appreciate help provided in MPI Chemie by U. Pöschl. We thank P. Alireza and G. Lonzarich for help with samples of CuTi; J. Kamarad, S. Toser and C. Q. Jin for sharing their experience on SQUID measurements; K. Shimizu and his group for cooperation; P. Chu and his group for many discussions and collaboration, and L. Pietronero, M. Calandra and T. Timusk for discussions. V.K. and S.I.S. acknowledge the DFG (Priority Program No. 1458) for support. M.I.E. thanks H. Musshof and R. Wittkowski for precision machining of the DACs.

Author Contributions A.P.D. performed the most of the experiments and contributed to the data interpretation and writing the manuscript. M.I.E. designed the study, wrote the major part of the manuscript, developed the DAC for SQUID measurements, and participated in the experiments. I.A.T. participated in experiments. V.K. and S.I.S. performed the magnetic susceptibility measurements and contributed to writing the manuscript. M.I.E. and A.P.D. contributed equally to this paper.

Author Information Reprints and permissions information is available at www.nature.com/reprints. The authors declare no competing financial interests. Readers are welcome to comment on the online version of the paper. Correspondence and requests for materials should be addressed to M.I.E. (m.eremets@mpic.de).

METHODS

Experimental procedure. For electrical measurements we used diamond anvil cells (DACs) with anvils of the following shape: tip diameter of 200–300 μm bevelled at 7–8° to a culet of 40–80 μm. An insulating gasket is required to separate the metallic gasket from the electrodes. It was prepared in the following way (Extended Data Fig. 3). First a metallic gasket of T301 stainless steel (or Re) 250 μm thick was indented with about 17–20 GPa pressure. Then the bottom of the imprint of diameter ~200 μm was drilled out, and a powder insulating material was put in the imprint and pressed between the anvils to form a layer. The insulating layer was made of either Teflon, NaCl or $CaSO_4$ as these materials do not react with H_2S. The layer was pressed to obtain a thickness in the centre of ~3–5 μm to provide stable clamping. A larger thickness leads to instability in the sample—it shifts or escapes under pressure—while with a thinner gasket it is difficult to reach high pressures. A hole of diameter ~10–30 μm was then drilled in the insulating layer. Four Ti electrodes were sputtered on the diamond anvil. The electrodes were capped with Au to prevent oxidation of the Ti. (To check a possible contribution of the diamond surface to the conductivity, we prepared a different configuration of electrodes for a once-only experiment: two electrodes were sputtered on one anvil and another two on another anvil, similar to ref. 13). After preparation of the electrodes the gasket was put back on the anvil and the DAC was assembled so that the separation between the anvils was about 20–100 μm (measured by interference fringes). The DAC was placed into a cryostat and cooled down to ~200 K (within the temperature range of liquid H_2S) and then H_2S gas was put through a capillary into a rim around the diamond anvil where it liquefied (Extended Data Fig. 4). H_2S of 99.5% and D_2S of 97% purity were been used. The filling was monitored visually (Extended Data Figs 4, 5) and the sample was identified by measuring Raman spectra. Then liquid H_2S was clamped in the gasket hole by pushing the piston of the DAC with the aid of screws outside the cryostat. The thickness of the sample can be estimated to be few micrometres, as measured from interference spectra through the clamped transparent sample. The thickness might be ~1 μm if the sample expanded over the culet (Fig. 4). After the clamping, the DAC was heated to ~220 K to evaporate the rest of the H_2S, and then the pressure was further increased at this temperature. The pressure remained stable during the cooling within ±5 GPa. The pressure was determined by a diamond edge scale at room temperature and low temperatures[32]. For optical measurements a Raman spectrometer was equipped with a nitrogen-cooled CCD and notch filters. The 632.8 nm line of a He–Ne laser was used to excite the Raman spectra and to determine pressure.

The low temperature loading seems to be required to prepare samples with high T_c. If H_2S was loaded at room temperature in the gas loader, for example, only sulfur was detected in Raman and X-ray scattering. Apparently in this route the sample decomposes before reaching the required high-pressure phase of H_3S. We did not explore all (P,T) paths to reach the state with high T_c. We found however that superconductivity is not observed in sample loaded at ~200 K but heated to room temperature at low pressure <~100 GPa.

The resistance and Raman spectra were measured during the pressurizing using the four-probe van der Pauw method (Extended Data Fig. 3) with a current of 10–10,000 μA. The temperature was reliably determined by using a slow warming rate (~1 K min^{-1}) and allowing the DAC to equilibrate with attached thermometer. The determined T_c was well reproduced in measurements with the PPMS6000 (Physical Property Measurement System from Quantum Design) and other set-ups. T_c was determined as the point of steepest change of resistance from the normal state (Fig. 2b).

The influence of the magnetic field on superconducting transitions has been measured with a non-magnetic DAC (diameter 25 mm) in a PPMS6000 in a 4–300 K temperature range and fields up to 7 T.

Magnetic susceptibility measurements were performed in an MPMS (Magnetic Property Measurement System) from Quantum Design. For these measurements a miniature non-magnetic cell made of Cu:Ti alloy working up to 200 GPa was designed (Fig. 4b). Samples of diameter ~50–100 μm and a thickness of a few micrometres were prepared to provide a sufficient signal. Magnetic susceptibility measurements using a high-pressure cell were performed using a background subtraction feature of the MPMS software of the SQUID magnetometer (Extended Data Fig. 6).

Results. We present here some important key features of our new high-T_c sulfur hydride superconductor:

(1) The new superconductor is of type II. This fact is clearly supported by (i) a difference in temperature-dependent ZFC and FC magnetization (Fig. 4a), which is due to the Meissner effect (ZFC) and magnetic flux capture when the sample is cooled down from its normal state (FC); and (ii) the magnetic hysteresis curves (Fig. 4c, d). The magnetic hysteresis curves also have all the features of typical type II superconductors with a mixed state between H_{c1} and H_{c2}.

(2) A typical value of the coherence length ξ_{GL} in the framework of the Ginzburg–Landau theory can be estimated on the basis of the measured upper critical fields from conductivity measurements (Fig. 3c). Using the experimental estimation 60 T < H_{c2} < 80 T and the relation

$$\xi_{GL} = \frac{1}{2}\sqrt{\frac{h}{\pi e H_{c2}}}$$

we find limits for the coherence length: 2.3 nm > ξ_{GL} > 2.0 nm. We note that this relatively short coherence length is of the same order as, for instance, the values for superconducting $YBa_2Cu_3O_7$ (1.3 nm) and Nb_3Sn (3.5 nm).

(3) The London penetration depth λ_L can be estimated from the known relation of the lower critical field H_{c1} to the upper critical field H_{c2} for a type II superconductor

$$\frac{H_{c1}}{H_{c2}} \approx \frac{\ln\kappa}{2\sqrt{2}\kappa^2}$$

in the limit $\kappa \gg 1$ of the Ginzburg–Landau parameter $\kappa = \frac{\lambda_L}{\xi_{GL}}$. Considering the experimental value of the first critical field of 3×10^{-2} T (Fig. 4c) and the above-mentioned relation 60 T < H_{c2} < 80 T, we can obtain the following estimate for the London penetration depth: $\lambda_L \approx 125$ nm.

(4) According to Bean's model, the magnetic critical current density of the superconductor can be estimated from the distance between the direct and the returning branches of the magnetic hysteresis loop at a given magnetic field (Fig. 4c). Provided grain radii are about 0.1 μm, the intra-grain critical current J_c is about 10^7 A cm^{-2}.

32. Eremets, M. I. Megabar high-pressure cells for Raman measurements. *J. Raman Spectrosc.* **34,** 515–518 (2003).
33. Landau, L. D. & Lifshitz, E. M. *Electrodynamics of Continuous Media* Vol. 8, 1st edn, 173 (Pergamon, 1960).

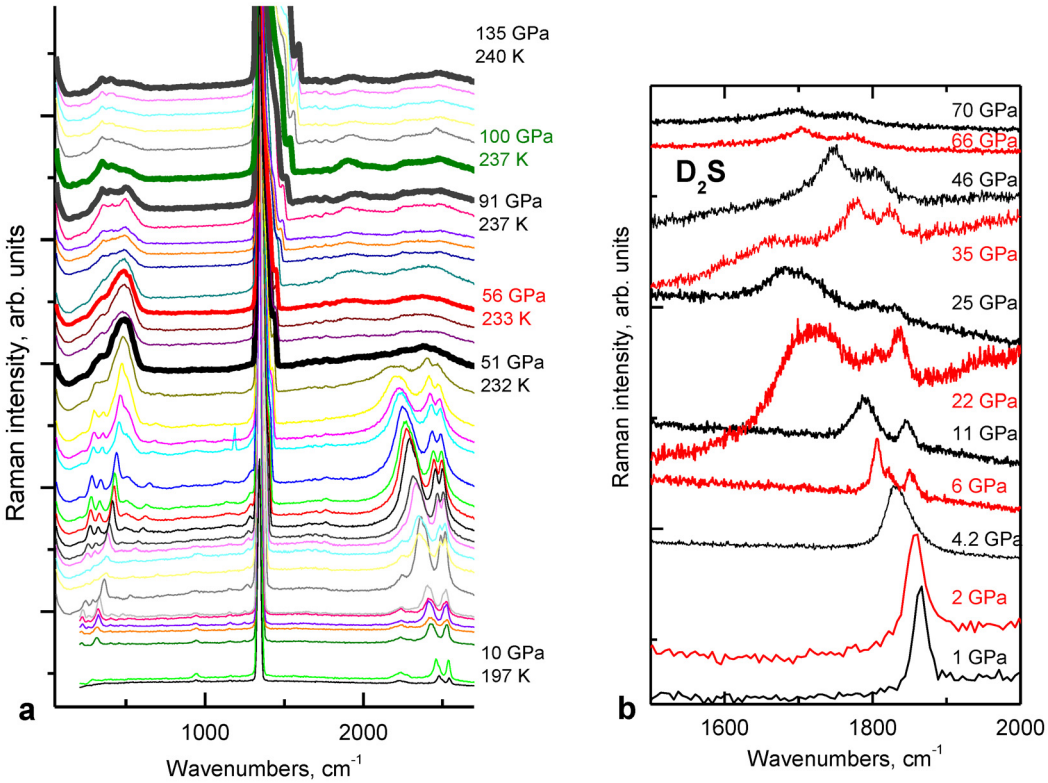

Extended Data Figure 1 | Raman spectra of sulfur hydride at different pressures. a, Spectra of sulfur hydride at increasing pressure at ~230 K. The spectra are shifted relative to each other. At 51 GPa there is a phase transformation, as follows from disappearance of the characteristic vibron peaks in the 2,100–2,500 cm^{-1} range. The corresponding spectrum is highlighted as a bold curve. Bold curves at higher pressure (and the temperature of the measurement) are shown to follow qualitatively the changes of the spectra. The pressure corresponding to the unassigned plots can be determined from the Raman spectra of the stressed diamond anvil[32]. **b**, Raman spectra of sulfur deuteride measured at $T \approx 170$ K and over the pressure range 1–70 GPa.

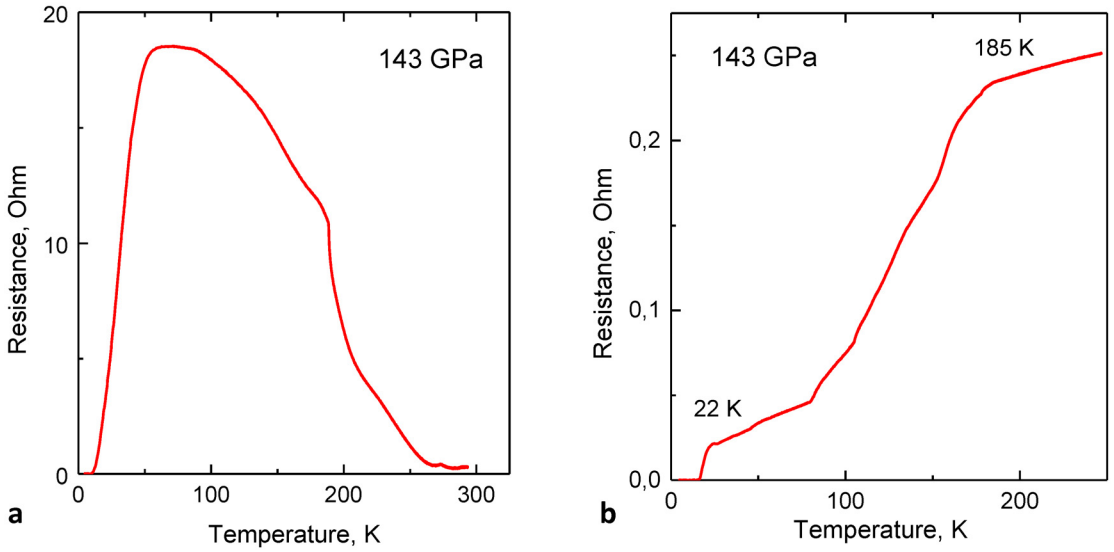

Extended Data Figure 2 | Temperature dependence of the resistance of sulfur hydride at 143 GPa. In this run the sample was clamped in the DAC at $T \approx 200$ K, and the pressure then increased to 103 GPa at this temperature; the further increase of pressure to 143 GPa was at ~100 K. **a**, After next cooling to ~15 K and subsequent warming, a superconducting transition with $T_c \approx 60$ K was observed, then the resistance strongly decreased with increasing temperature. After successive cooling and warming (**b**; only the warming curve is shown) a kink at 185 K appeared, indicating the onset of superconductivity. The superconducting transition is very broad: resistance dropped to zero only at ~22 K. There are apparent 'oscillations' on the slope. Their origin is not clear, though they probably reflect inhomogeneity of the sample in the transient state before complete annealing. Similar 'oscillations' have also been observed for other samples (see, for example, figure 3 in the Supplementary Information of ref. 9).

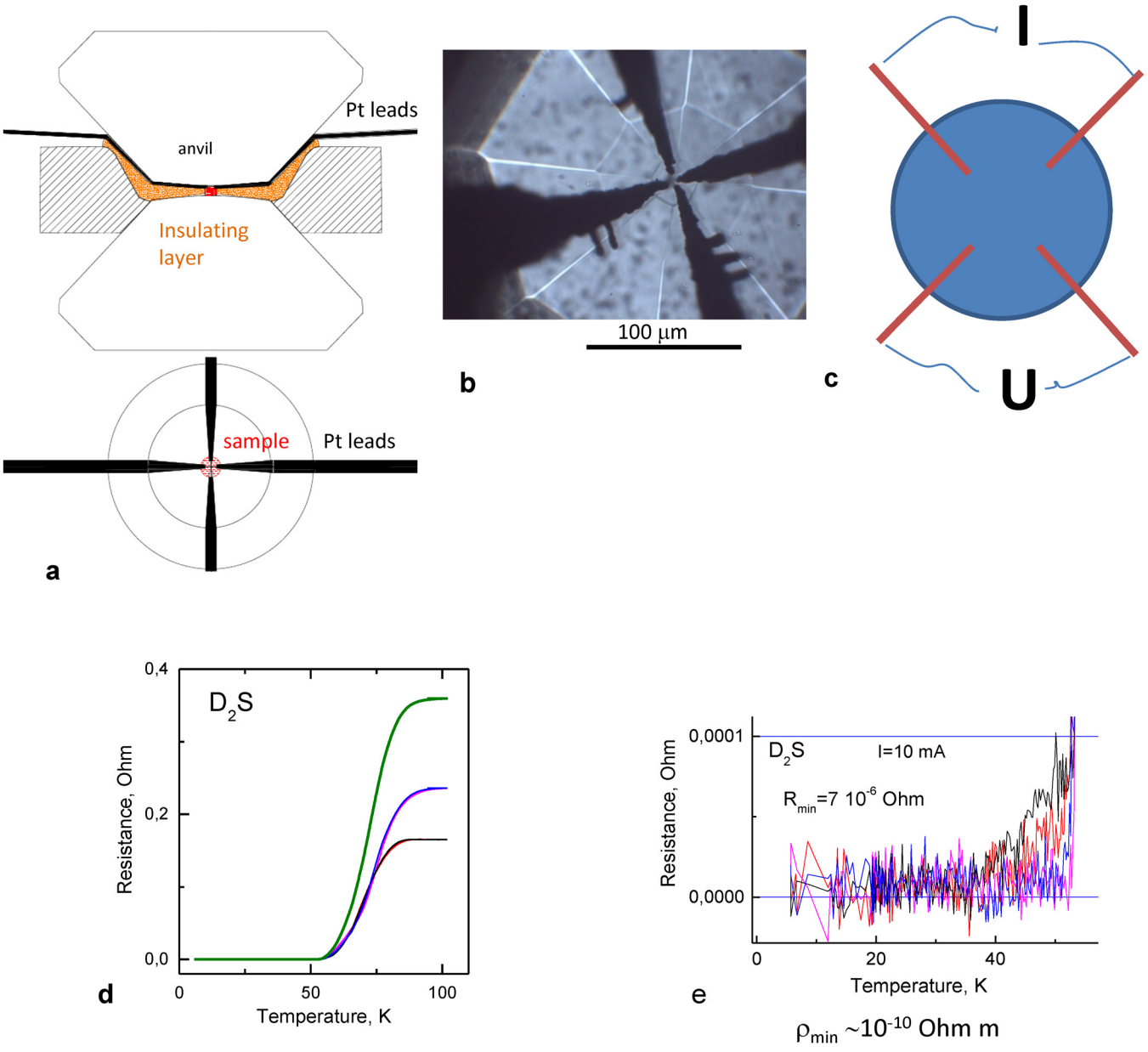

Extended Data Figure 3 | Electrical measurements. **a**, Schematic drawing of diamond anvils with electrical leads separated from the metallic gasket by an insulating layer (shown orange). **b**, Ti electrodes sputtered on a diamond anvil shown in transmitted light. **c**, Scheme of the van der Pauw measurements: current leads are indicated by *I*, and voltage leads as *U*. **d**, Typical superconducting step measured in four channels (for different combinations of current and voltage leads shown in **c**). A sum resistance obtained from the van der Pauw formula is shown by the green line. Note here that the superconducting transition was measured with the un-annealed sample[9]. After warming to room temperature and successive cooling, T_c should increase. **e**, Residual resistance measured below the superconducting transition (**d**). R_{min} and ρ_{min} are averaged over four channels shown by different colours.

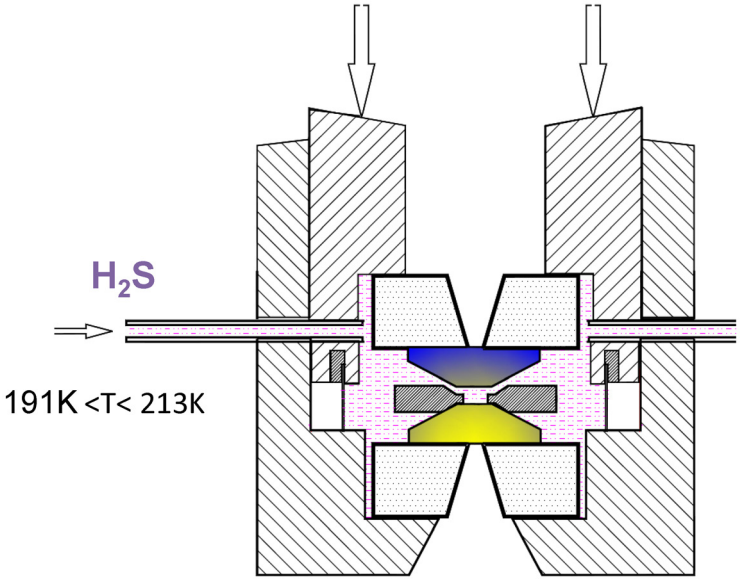

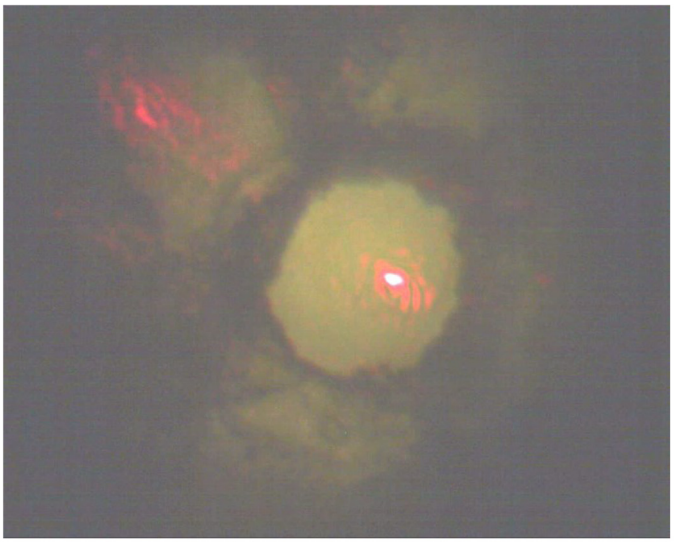

Extended Data Figure 4 | Loading of H_2S. Gaseous H_2S is passed through the capillary into a rim around the diamond anvils (upper panel). When the sample liquefies, in the temperature range 191 K $< T <$ 213 K, it is clamped. The process of loading is shown on a video (https://vimeo.com/131914556) and a still is shown here (lower panel). On the video, the camera is looking through a hole in the transparent gasket ($CaSO_4$), and shows a view through the diamond anvil. At $T \approx$ 200 K, the line to the H_2S gas cylinder was opened and the gas condensed. At this moment, the picture changes due to the different refractive index of H_2S. The second anvil with the sputtered electrodes was then pushed forward, and the hole was clamped. The sample changed colour during the next application of pressure. The red point is from the focused HeNe laser beam.

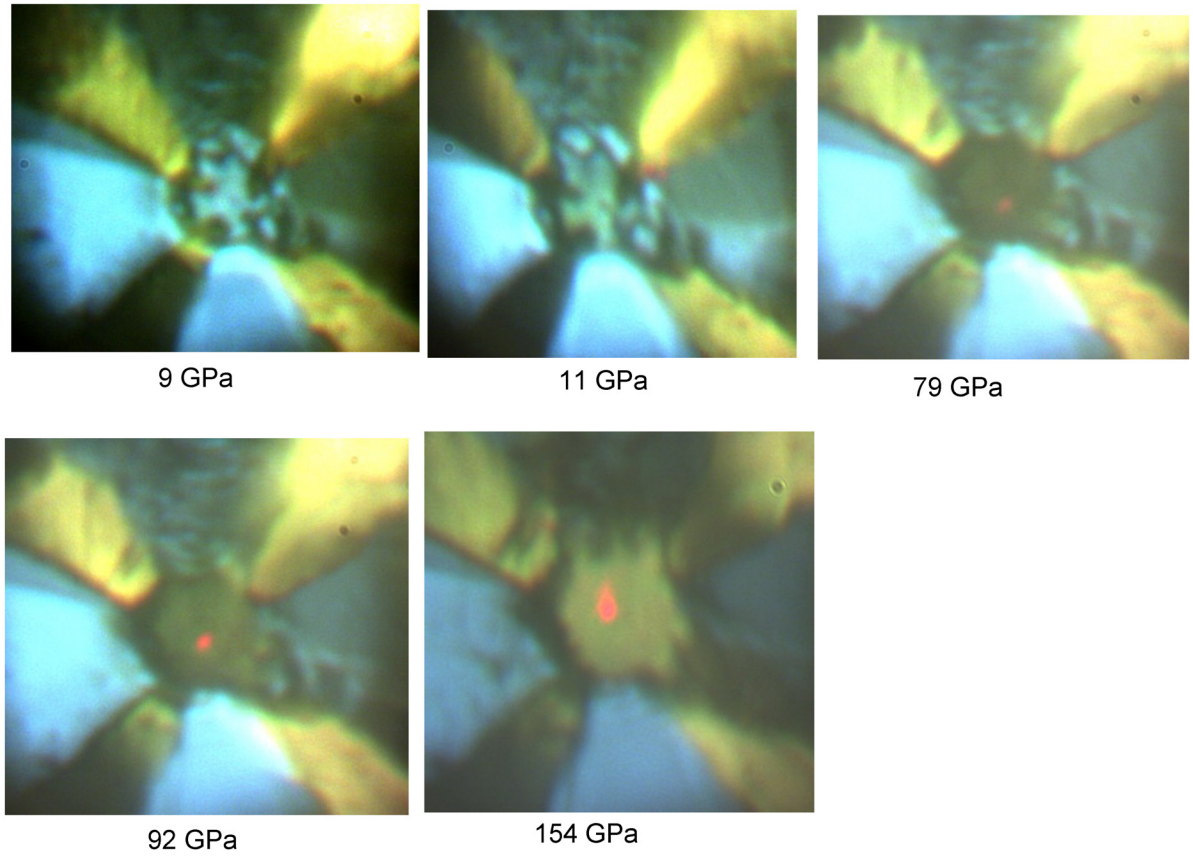

Extended Data Figure 5 | View of D_2S sample with electrical leads and transparent gasket ($CaSO_4$) at different pressures. The D_2S is in the centre of these photographs, which were taken in a cryostat at 220 K with mixed illumination, both transmitted and reflected. Under this illumination, the insulating transparent gasket shows blue, and the electrodes yellow. The red spot is the focused HeNe laser beam. The sample, which is initially transparent, becomes opaque and then reflective as pressure is increased.

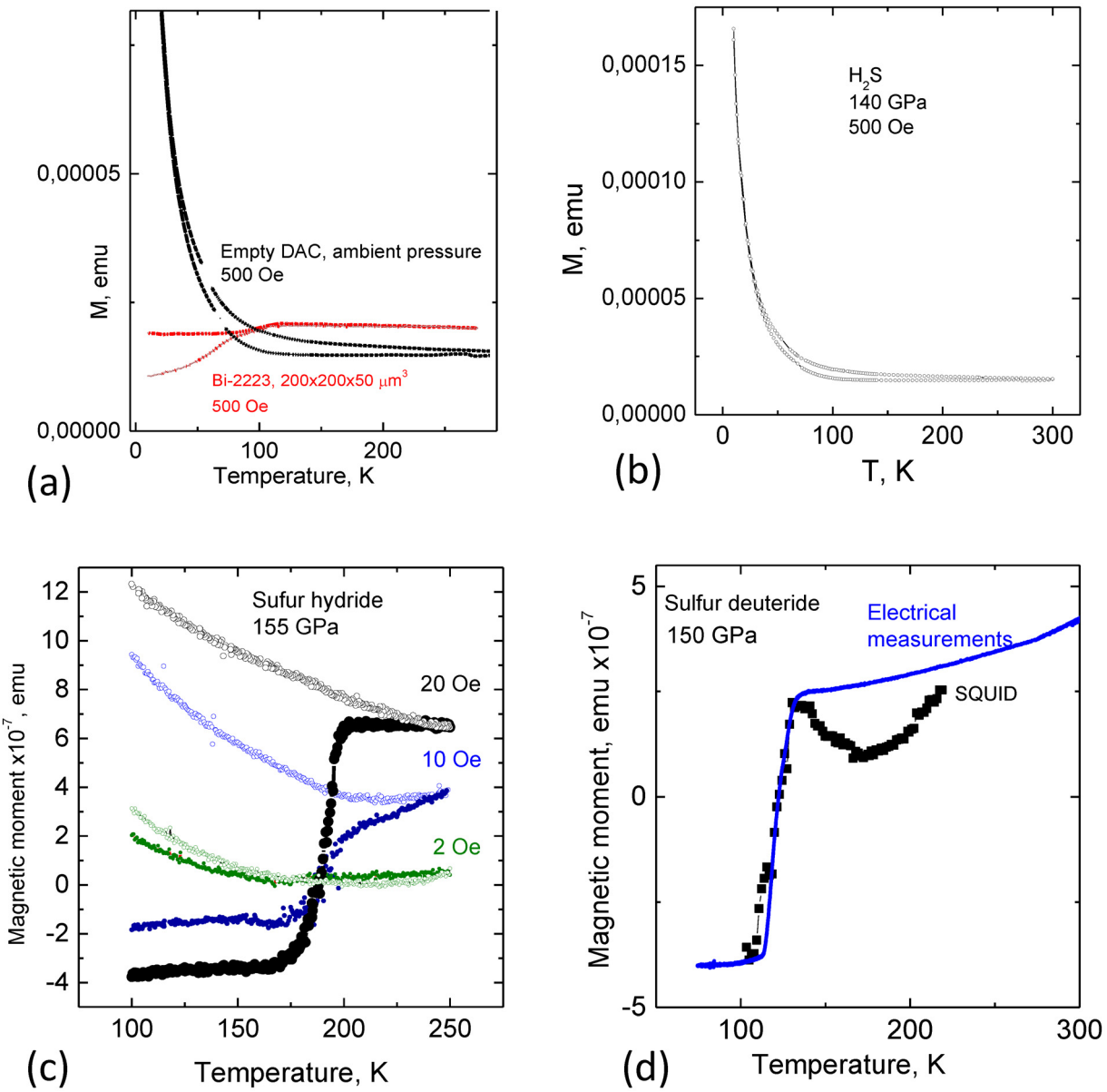

Extended Data Figure 6 | Magnetic susceptibility measurements with a SQUID. A typical sample (Fig. 4) has a disk shape (diameter 50–100 μm and thickness of few micrometres). In the superconductive state the magnetic moment for this disk is estimated as $M(\text{disk}) \approx 0.2r^3H$ (ref. 33). For a disk of radius $r = 40$ μm (a sample size typical for DACs in the megabar range) and $H = 2$ mT the expected diamagnetic signal, M(disk) is estimated as 2.6×10^{-7} emu. This value is well above the sensitivity of the SQUID which is $\sim 10^{-8}$ emu and, therefore, the signal can be detected. A high-pressure DAC made of Cu:Ti alloy has its own magnetic background signal (**a**) which increases sharply at low temperatures due to residual paramagnetic impurities. Signal from a large superconducting sample (for example, a Bi-2223 superconductor) could still be detected without magnetic background subtraction. However, the sulfur hydride sample is not seen (**b**) unless background has been subtracted (**c**, **d**). The background signal acquired in the normal state immediately above T_{onset} has been used for subtraction over all the temperature range taking into account that the magnetic moment of the DAC is fairly temperature independent above 100 K. **c**, Magnetic measurements for the sample of sulfur hydride at different magnetic fields (labels on curves). The data on sulfur deuteride (**d**) are compared with the superconducting transition in resistivity measurements (blue curve) which has been scaled to fit the susceptibility data (black points).